

Investigation of second phase concentration effects on tribological and electrical properties of Cu-WS₂ composites

Marco Freschi¹, Matteo Di Virgilio^{1,*}, Oskari Haiko², Marco Mariani³, Luca Andena¹, Nora Lecis³,
Jukka Kömi², Giovanni Dotelli¹

¹ → Department of Chemistry, Materials and Chemical Engineering “Giulio Natta”, Politecnico di Milano, Piazza Leonardo Da Vinci 32, 20133 Milano, Italy

² → Materials and Mechanical Engineering, Centre for Advanced Steels Research, University of Oulu, Pentti Kaiteran katu 1, 90570 Oulu, Finland

³ → Department of Mechanical Engineering, Politecnico di Milano, Via La Masa 1, 20156 Milano, Italy

e-mail addresses: marco.freschi@polimi.it
 matteo.divirgilio@polimi.it
 oskari.haiko@oulu.fi
 marco.mariani@polimi.it
 luca.andena@polimi.it
 nora.lecis@polimi.it
 jukka.komi@oulu.fi
 giovanni.dotelli@polimi.it

*Corresponding author: Matteo Di Virgilio, matteo.divirgilio@polimi.it, tel. +39 02 2399 3232

Abstract: In this preliminary study, a set of self-lubricating copper-tungsten disulfide (Cu-WS₂) composites are prepared via a powder metallurgy route to analyze the effects of solid lubricant concentration on their tribological, electrical and wettability properties. An extensive characterization is performed to preliminarily assess the potential application of these metal matrix composites (MMCs) in sliding electrical contacts working under harsh conditions. The experimental results reveal the beneficial effect of WS₂ on the wear behavior of the prepared composites, as demonstrated by friction coefficient, specific wear rate and wear coefficients results. A second phase content in the 10–15 wt % range appears to guarantee the better combination of the desired features.

Keywords: metal matrix composites, solid lubricants, wear mechanism, tribology

1. Introduction

Sliding electrical contacts are electrical junctions between moving (e.g. rotating) and stationary conductors through which power and signals can flow, allowing the continuity of a circuit [1,2]. Regardless of sliding electrical contact configuration, all the assemblies consist of brushes that slip on rings [3]. They are critical components in a wide range of devices, such as commutators for direct current (DC) electromotors in the automotive field, alternators, slip rings for aerospace applications, wind turbines, chip-mounters, micro-computers, and household appliances [4,5]. Copper alloys are used for large current rings, whereas silver and its alloys are preferred when resistance to the formation of hard oxides and to sulfur-containing species is required. Gold or gold alloys are also considered, as they are inert in the atmospheric environment, and they have low catalytic activity in reactions involving organic gases. Generally, silver or gold plating are used as a cladding or electroplate on a bulk metal to reduce the overall cost [5]. Carbon graphite has been historically the primary material employed for brushes, since its crystallographic structure presents weak interlayer van der Waals bonds that encourage lamellar sliding. Electrographite is its direct improvement, in as much it is enriched by a suitable amount of hard particles which assure an acceptable combination between mechanical strength and electrical conductivity. A similar result can be obtained via the combination with metals or resins to give the so-called metal graphite and resin-bonded graphite [4,6]. However, some criticalities arise with carbon-based brushes: the inherently high electrical resistivity, which may implicate an undesired generation of waste heat; the scarce system compliance and lifetime of monolithic members; the limited ability to work with rough rotor surfaces, especially at high speed; the one order of magnitude higher-drop in electrical potential of graphite-metal sliding contacts with respect to metal-metal ones [6]. Furthermore, the overall performance is intimately tied to the friction and wear phenomena occurring at the interface between the two components in contact. Precious metals, their alloys and copper-based reinforced composites have recently demonstrated worth of further insights for low-voltage and small-current applications due to stable low contact resistance and a reduced wear rate [5]. This last feature becomes imperative for those particular cases

in which the reliability of electrical contact must be preserved over long periods, thus limiting required maintenance operations. To further improve the minimization of the wear rate, suitable lubrication is of paramount importance, hence it represents the technical challenge currently addressed by most of the research in this field [7–13]. Solid lubricants technology is rapidly advancing, as they typically own a layered molecular structure of tightly bound atoms that bestows aptitude for sliding and a noteworthy shear resistance. Therefore, they are capable to promote the formation of a thin tribo-film between contacting materials. In such way, optimal low friction and low wear conditions in the specific operating environment can be achieved [8,14]. Graphite, graphene nanoplatelets (GNP) and transition metal dichalcogenides (TMDs) are the primary exponents of these fascinating materials. Two-phase metal matrix composites (MMCs) are typically obtained by coupling a compatible metal matrix, such as copper, with one of these lamellar solids. Conversely, multi-phase MMCs are fabricated by employing two or more different solid lubricants. In both cases, the final array of properties of an MMC blends those of the single phases while conserving their chemical and physical individuality [15]. One of the most widespread techniques to produce MMCs is powder metallurgy (PM), which includes a milling step aimed to favor the solid lubricant's dispersion in the matrix and to discourage unwanted particles' agglomeration.

TMDs are receiving considerable attention as dispersed solid lubricants in MMCs. They are a family of compounds characterized by a general formula TX_2 , in which T is a transition metal, such as molybdenum (Mo) or tungsten (W), and X represents a chalcogen, such as sulfur (S), selenium (Se) or tellurium (Te). Amongst them, molybdenum disulfide (MoS_2) and tungsten disulfide (WS_2) are drawing attention to improve the tribological features of particle-reinforced copper-based composites [13,16–20]. They exhibit the typical anisotropic quasi two-dimensional crystal structure of TMDs, comprised of a middle plane of metal atoms sandwiched between two layers of chalcogen atoms [8,21]. The intra-layer bonds are covalent, whereas the inter-layer ones, between adjacent sandwiches, are relatively weak van der Waals forces. Therefore, layers can easily slide when shearing forces are applied. The subsequent generation of a tribo-film on the worn surface, through the continuous supply

of lubricant, strongly reduces friction coefficient and wear rate. WS₂ is characterized by chemical inertness, stability to oxidation, powder dispersibility, long service life and an excellent thermal resistance, demonstrated by a 730 °C-maximum operating temperature which is about 100°C higher than that of MoS₂ [16,22]. However, it is more expensive and therefore slightly less competitive than MoS₂ in conventional applications, hence its employment is preferred in those sectors (e.g., aerospace) in which sliding electrical contacts operate under more extreme conditions.

A consistent research effort is being produced to deeply understand and improve the characteristics of copper-tungsten disulfide (Cu-WS₂) composites, with authors focalizing on various parameters of a typical preparation procedure. Zhao et al. [18] have characterized copper-tungsten disulfide composites with variable WS₂ content from 5 to 30 vol %, prepared via spark plasma sintering (SPS), observing a strong improvement in tribological properties. The sample containing 25 vol % of WS₂ has provided the best performance, with a friction coefficient of 0.16 and specific wear rate of $5 \times 10^{-5} \text{ mm}^3 \text{ N}^{-1} \text{ m}^{-1}$. The authors have verified the formation of an overall 60 nm-thick tribo-film composed of a thinner oxygen-rich layer and a thicker copper sulfide (Cu₂S)-rich one, whose presence has directly affected the friction and wear behavior by impeding the contact between studied composites and the counter ball during wear tests. Xiao et al. [19] have fabricated Cu-WS₂ composites with a solid lubricant's content up to 40 vol % by hot-pressing (HP). Tribological testing has allowed to monitor a remarkable reduction of the friction coefficient and to identify delamination wear as the main wear mechanism, with WS₂ layers arranging horizontally in the tribo-film. Differently from other species such as graphite [24], Cu-WS₂ composites have revealed a higher Vickers hardness (up to 94.7 HV) than pure copper (75.4 HV). The annealing of the samples at different temperatures from 700 to 950 °C has demonstrated a progressive accentuation of the decomposition of tungsten disulfide and the undesired formation of Cu₂S, with a consequent worsening of the tribological performance. Zhou et al. [20] have analyzed the effect of different grain sizes (0.6 and 5.0 μm) of WS₂ particles on the mechanical and tribological properties of Cu-WS₂ composites with a 20 wt %-content of lubricating phase. Although both composites have showed self-lubricating properties, the specimen

containing larger particles has displayed higher bending strength (292.2 vs 181.5 MPa), higher Brinell hardness (96.3 vs 91.1 HB), lower friction coefficient (0.158 vs 0.172) and lower wear rate (2.99×10^{-5} vs $6.13 \times 10^{-5} \text{ mm}^3 \text{ N}^{-1} \text{ m}^{-1}$). This discrepancy has been attributed to the higher bonding strength that larger WS₂ particles exhibit with the copper matrix, able to favor the generation and a longer propagation of microcracks at the phase interface. Moreover, the smoother transfer film, the lower concentration of tribo-oxidation products and the smaller wear debris observed in the composite with 5.0 μm WS₂ particles have contributed to its better wear resistance. Wang et al. [25] have reported differences in friction coefficient of Cu-WS₂ composites depending on the production method: samples manufactured through HP have displayed an approximately halved friction coefficient (≈ 0.20) with respect to samples prepared via SPS (≈ 0.40). Concerning hardness and wear rate, values of the same order have been measured regardless of the exploited technique.

This work aspires to investigate the effects of a fundamental aspect of the preparation of self-lubricating Cu-WS₂ tablets, namely the tungsten disulfide content. From previous studies of our research group [26], promising results have been obtained for a 10 wt %-concentration of WS₂. Therefore, a set of composites with progressive 5 wt %-increase in WS₂ content ranging from 5 wt % to 30 wt % has been prepared while considering the one connoted by a 10 wt % of WS₂ as a benchmark. PM has been selected as the most reliable production technique, as it combines affordability and process simplicity. Firstly, the ball milling step has been executed to properly mix, grind, and homogenize the metal matrix and the solid lubricant powders. Then, powder compaction and tableting has been achieved via cold pressing. In the end, solid-state pressureless sintering has allowed to further increase density and mechanical strength of the manufactured tablets. Granulometry tests, X-ray diffraction (XRD), static optical contact angle (OCA) measurements, scanning electron microscopy (SEM), density evaluation, electrical properties assessment, indentation hardness tests, micro-scratch tests, wear tests and laser confocal scanning microscopy have been exploited to perform an extensive characterization of the prepared samples, in order to

ascertain their electrical, mechanical and tribological properties and, consequently, their potential practicability in sliding electrical contacts working under harsh conditions.

2. Materials and Methods

2.1 Materials

Electrolytic copper powders with a nominal particle size of 45 μm and a purity level $> 99.5\%$ have been acquired from Makin Metal Powders (Rochdale, UK). Sigma-Aldrich Corporation (St. Louis, MO, USA) has supplied tungsten disulfide micro-powders with a mean particle size of 2 μm and a purity of 99%. Copper powders have been initially dried in oven (G-2100, F.LLI GALLI G. & P. snc, Fizzonasco di Pieve Emanuele, Italy) at 120 $^{\circ}\text{C}$ for 6 hours to remove residual moisture. A 1-level roller ball milling system (MGS S.r.l., Olginate, Italy) has been employed to mix and grind Cu and WS_2 powders, in order to obtain a homogenous dispersion with smaller particles. Powders have been placed inside a polyethylene (PE) container together with 15-mm diameter zirconia (ZrO_2) spheres with a 10-to-1 ball-to-powder weight ratio (BPR). The container has been in turn inserted in a cylindrical porcelain alumina jar, which has been rolled on the mill at 60 rpm for 2 hours. Powder compaction and tableting has been achieved via cold-pressing: 1.5 g of milled powder have been introduced into a steel tablet-making device and subjected to a 6 tons-pressure for five minutes by means of hydraulic press (Specac Ltd., Orpington, UK), to obtain tablets characterized by a 13 mm-diameter and a thickness of roughly 2 mm. Afterwards, samples have undergone a sintering process in a EHA Model 1200 $^{\circ}\text{C}$ E-Range Tube Furnace (Carbolite Gero Ltd., Hope, UK) equipped with a thermocouple, to check the temperature of the 6 cm-diameter ceramic inner tube, and two Brooks[®] Instrument (Hatfield, PA, USA) Smart Mass Flow Controller 5850, to guarantee a flow atmosphere of 95% N_2 and 5% H_2 . A heating rate of 8 $^{\circ}\text{C min}^{-1}$ has been applied up to a temperature of 550 $^{\circ}\text{C}$, which has been maintained for one hour. This specific value has been chosen to avoid thermal decomposition of the lubricating agent, determined from previous thermogravimetric analyses on

pure WS₂ powders. In the end, the treated tablets have been naturally cooled down in the process environment.

This procedure has been employed to fabricate a set of five self-lubricating composites with WS₂ concentrations of 5, 15, 20, 25 and 30 wt %. The samples have been denominated Cu-XWS₂, in which X represents the lubricant mass content. Furthermore, the promising composite with 10 wt %-content of WS₂, previously investigated by our research group [26], has been considered as a benchmark and subjected to additional analyses to perform a complete comparison and to better understand the effects of the second phase content on the features of copper matrix composites. Due to the commonality of the raw materials batches and to be consistent with the above-mentioned designation, the benchmark sample has been recognized as Cu-10WS₂.

2.2 Granulometry tests

Granulometry tests have been performed on the milled powders by means of the Particle Size Analyzer CILAS 1180 L (CILAS SA, Orléans, France), which combines laser diffraction with a CCD camera to measure both fine and coarse particles in the dimensional range between 0.04 and 2500 μm.

2.3 X-ray diffraction analysis

X-ray diffraction (XRD) has been executed via the diffractometer D8 Advance (Bruker Corporation, Billerica, MA, USA), by employing a Cu-Kα filament to emit X-rays with a wavelength of 1.54 Å. A scanning rate of 0.02° per second in the angular interval of 5–90°, an applied tension of 40 kV, an applied current of 40 mA and a count time of one second have been set up as operating parameters during the experiments.

2.4 Optical contact angle measurements

The OCA 15plus (DataPhysics Instruments GmbH, Filderstadt, Germany), equipped with a 752x582 pixels-resolution CCD video-camera and supported by the image processing software SCA 20, has allowed to obtain static optical contact angle (OCA) measurements via a sessile drop method.

2.5 Scanning electron microscopy

The scanning electron microscope model Stereoscan 360 (Cambridge Scientific Instrument Company, London, UK) has been used to acquire micrographs of the samples polished cross-sections at 500x, 1000x and 3000x magnifications.

2.6 Density measurements

Density assessments have required the hydrostatic balance YDK01 (Sartorius AG, Göttingen, Germany), which enables to weigh the specimens both in air and in water. Absolute density of the composites, identified as δ (g cm⁻³), has been derived exploiting the Archimedes' principle through Eq. (1):

$$\delta = \frac{m_a \delta_w}{m_a - m_w} \quad (1)$$

in which m_a is the mass in air (g), δ_w is the density of water (g cm⁻³) and m_w is the mass of the solid completely immersed in the solvent (g). Considering the tabulated density of pure copper (δ_{Cu}), equal to 8.96 g cm⁻³ [27], the corresponding relative densities (δ_r , %) of the samples have been determined via Eq. (2):

$$\delta_r = 100 \frac{\delta}{\delta_{Cu}} \quad (2)$$

2.7 Electrical properties evaluation

The DC resistance-meter model 2841 (B&K Precision Corporation, Yorba Linda, CA, USA) has been employed to measure the electrical resistance of each composite. The dependence of the resistance values to the geometrical conformation of the analyzed samples has been minimized by exploiting two different measurement configurations. In the first one, test clips have been positioned at the edges of the tablet to maximize their distance. The second one has been attained by shifting one clip towards the central section of the specimen. The corresponding electrical resistivity ρ (Ω m) has been calculated through the second Ohm's law, reported in Eq. (3), in which R is the surveyed resistance

(Ω), t is the thickness of the tablet (m), l is the length (m) of the chord perpendicular to the inter-distance, d (m), and placed halfway between the two clips (Fig. 1):

$$\rho = \frac{R t l}{d} \quad (3)$$

The geometrical parameters have been manually assessed with a Fujisan digital micrometer.

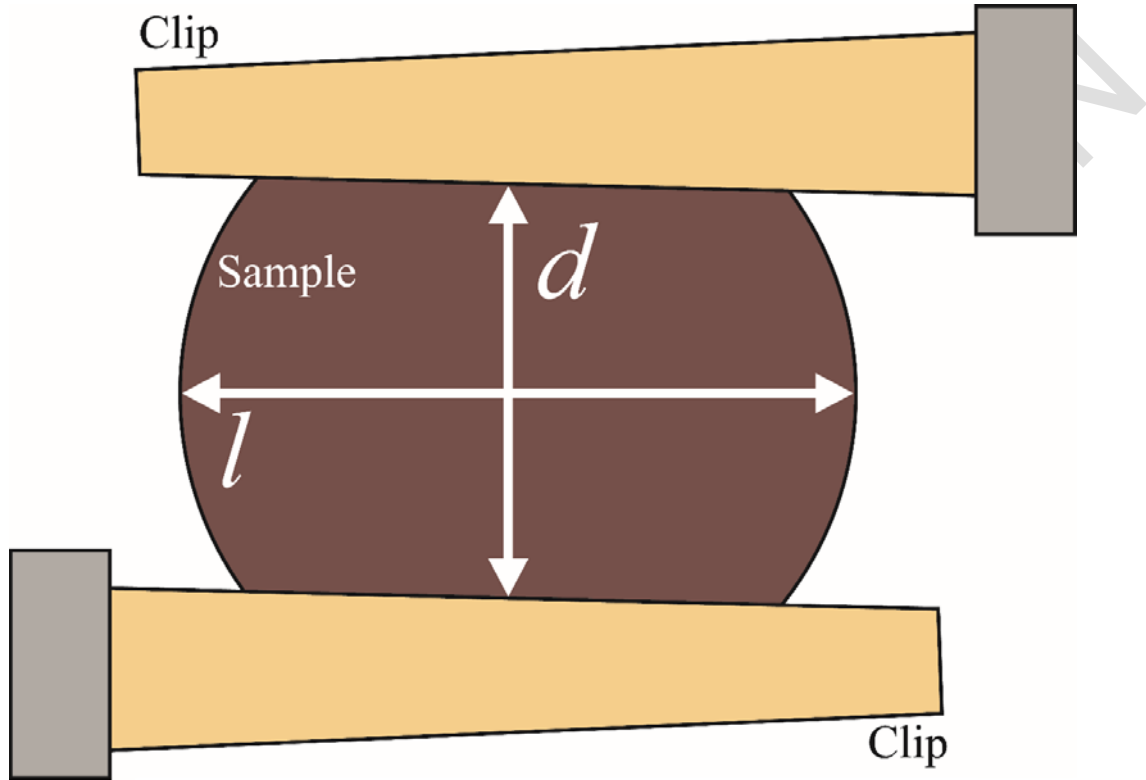


Fig. 1 Sketch of the geometrical parameters used to determine the electrical resistivity of the Cu-XWS₂ composites.

2.8 Scratch tests

Micro-scratch tests have been executed by means of the Micro-Scratch Tester provided by CSM Instruments (now Anton Paar TriTec SA, Corcelles, Switzerland). It is equipped with a conical Rockwell stainless steel indenter with a 200 μm -radius spherical diamond tip. A pre-scan and a post-scan stage have been performed with the lowest normal load (0.03 N) to correct measurements for the initial profile and measure the residual depth (R_d , mm) after scratching. The actual scratch stage has been completed by applying a normal load (F_n) of 15 N at a constant speed of 20 mm min⁻¹ for a length l_s equal to 3 mm, in order to record the evolution of the tangential force (F_t , N) and the

penetration depth (P_d , mm). A total of six suitable measurements for each specimen has been extrapolated from a set of ten scratches by discarding outliers. The parameters directly acquired from the experiments have enabled the evaluation of the apparent friction coefficient (FC) and scratch hardness (H_s , MPa) values. Friction coefficient has been computed through Eq. (4) as the ratio between the actual tangential force and the actual normal force:

$$FC = \frac{F_t}{F_n} \quad (4)$$

FC values so calculated combine two different components, originated by adhesion and deformation [28]; the deformation component can be quite high in scratch tests, therefore FC values cannot be directly compared with friction measurements performed during wear testing (in which tribo-film formation can also play a dominant role).

Eq. (5) has allowed to estimate scratch hardness as the ratio between the actual normal force and the normally projected contact area (A_c , mm²) [28,29]:

$$H_s = \frac{F_n}{A_c} \quad (5)$$

Considering the indenter's spherical tip, contact area has been assumed as that of a half circle [31], whose contact radius has been evaluated from the geometry of the tip and the penetration depth.

2.9 Indentation hardness tests

Indentation hardness tests have been carried out through the Microhardness Tester FM700 (TECMET 2000 S.r.l., Corsico, Italy). The instrument includes a square based pyramid as indenter, characterized by an angle (θ) of 136° between the opposite faces of the pyramid. Eq. (6) has permitted the computation of Vickers hardness (HV) values as average of three different estimations:

$$HV = \frac{2P \sin\left(\frac{\theta}{2}\right)}{L^2} \quad (6)$$

where P is the applied load of 4.9 N and L is the average length (mm) of the diagonal left by the indenter on the samples.

2.10 Wear tests

Wear tests have been conducted by means of a CSM Instruments (now Anton Paar TriTec SA, Corcelles, Switzerland) tribometer, implementing a ball-on-disk configuration. A 100Cr6 steel counter ball, connoted by a diameter of 6 mm and a hardness of 831 ± 21 HV, has been selected to effectively probe the softer copper-based composites without excessively deform or crash them. The normal load (F_n) acting on the ball has been fixed to 5 N. The tablets have been fastened to a mandrel and rotated at a controlled tangential speed of 0.18 m s^{-1} . In such way, the counter ball has produced a circular trail of radius 4.5 mm by covering an overall distance (d) of 500 m. Each test has been made under room temperature and atmosphere. The evolution of the prepared materials' friction coefficient has been considered as a function of the covered distance to infer their wear behavior. The optical microscope (OM) Eclipse LV150NL (Nikon, Tokyo, Japan) has allowed to examine the wear tracks of the composites at 25x and 50x magnifications. The scanning electron microscope EVO 50 EP/LZ4 PENTAFET (Carl Zeiss S.p.A., Oberkochen, Germany) has been chosen to check the wear tracks' surfaces at 400x and 1500x magnifications and the corresponding cross-sections at 20000x magnification.

2.11 Laser confocal scanning microscopy

The laser confocal scanning microscope model VK-X200 by Keyence Corporation, Osaka, Japan, has been employed to inspect the specimens subjected to scratch and wear tests, with the aim of appraising their morphology and wear deformation. The software VK Analyzer Plus has permitted the geometrical inspection of the wear groove and the residual material plastically displaced at the edges, as reported in Fig. 2. Volumetric wear losses W_v (mm^3) have been computed via Eq. (7) [32]:

$$W_v = (A_g - A_{dm}) l \quad (7)$$

In both equations, A_g and A_{dm} correspond to the cross-sectional area (mm^2) of the groove and of the total displaced material, respectively. The length l (mm) represents scratch length l_s for the scratches, and the track circumference C for the wear tracks. The corresponding specific wear rates W ($\text{mm}^3 \text{ N}^{-1}$

¹ m⁻¹) have been obtained (Eq. (8)) dividing the volumetric losses by the specific sliding distance s_d (m), 0.003 m for scratch tests and 500 m for wear tests, and the applied normal load F_n (N), 15 N for scratch tests and 5 N for wear tests:

$$W = \frac{W_v}{s_d F_n} \quad (8)$$

The Archard model can be expressed through Eq. (9) [32,33]:

$$\frac{W_v}{s_d F_n} = \frac{k}{H} \quad (9)$$

in which H (MPa) is scratch hardness (H_s) and Vickers hardness (HV) for scratch and wear tests, respectively, whereas k is the dimensionless wear coefficient. This parameter has been directly estimated for both scratch tests and wear tests combining Eq. (7), Eq. (8), and Eq. (9) to obtain Eq. (10):

$$k = \frac{(A_g - A_{dm}) l H}{s_d F_n} \quad (10)$$

of the Cu-XWS₂ composites.

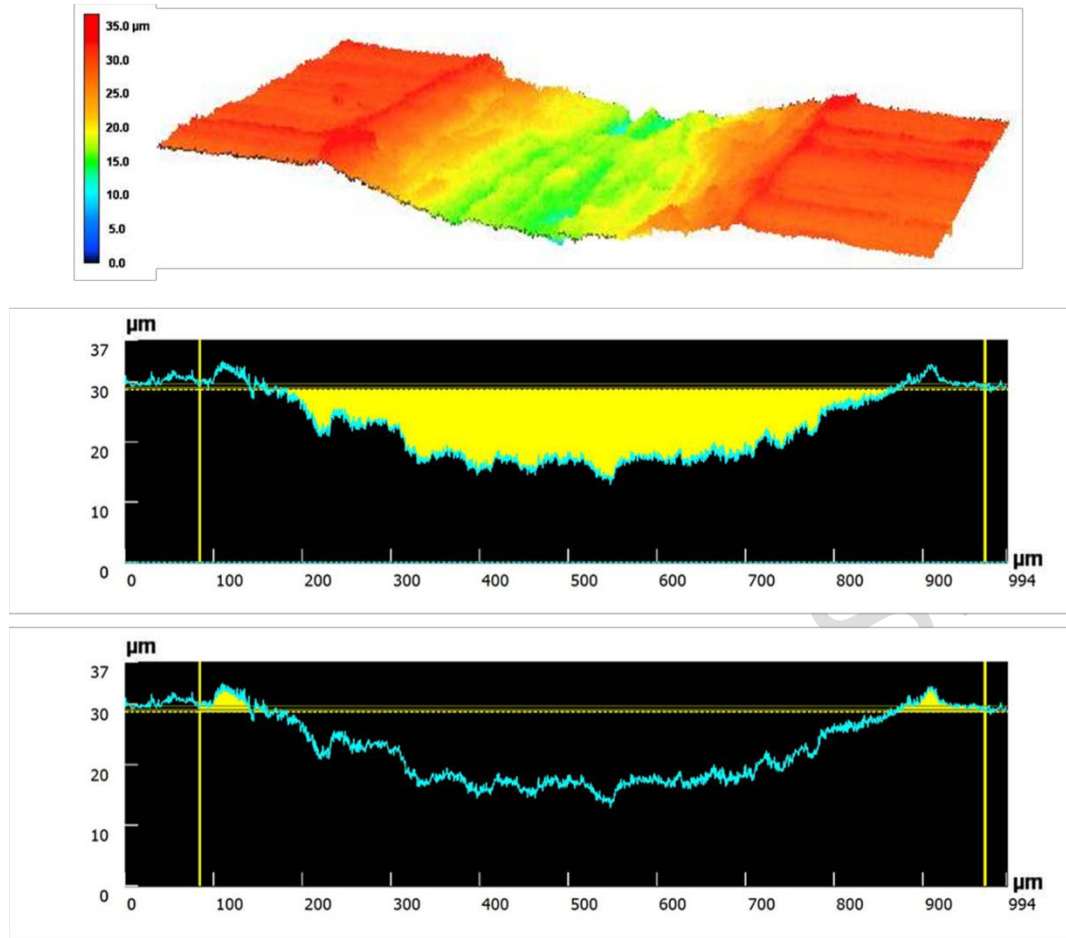


Fig. 2 Example of wear track profile analysis to evaluate the groove and the displaced material cross-sections.

3. Results and discussion

3.1 Granulometry

Fig. 3 displays the particle size distributions of Cu and Cu-XWS₂ powders. The distribution curves are rather broad, indicating an effective mixing and grinding process [34,35]. Nonetheless, some differences can be spotted with the increase of lubricant amount. Similar to Cu-10WS₂, Cu-5WS₂ and Cu-15WS₂ show narrower monomodal distributions with a modal diameter of 15, 16 and 17 μm respectively. Cu-20WS₂ reports a slight increase in distribution width and a tendency towards bimodality, as the main contributions are represented by particles with diameters of 8 and 17 μm. This behavior is further emphasized in Cu-25WS₂ and Cu-30WS₂, whose distributions are characterized by an increase of particles with similar dimension in the 8–17 μm range. The increase

of solid lubricant content determines a more pronounced presence of particles with diameter close to $0.6\ \mu\text{m}$.

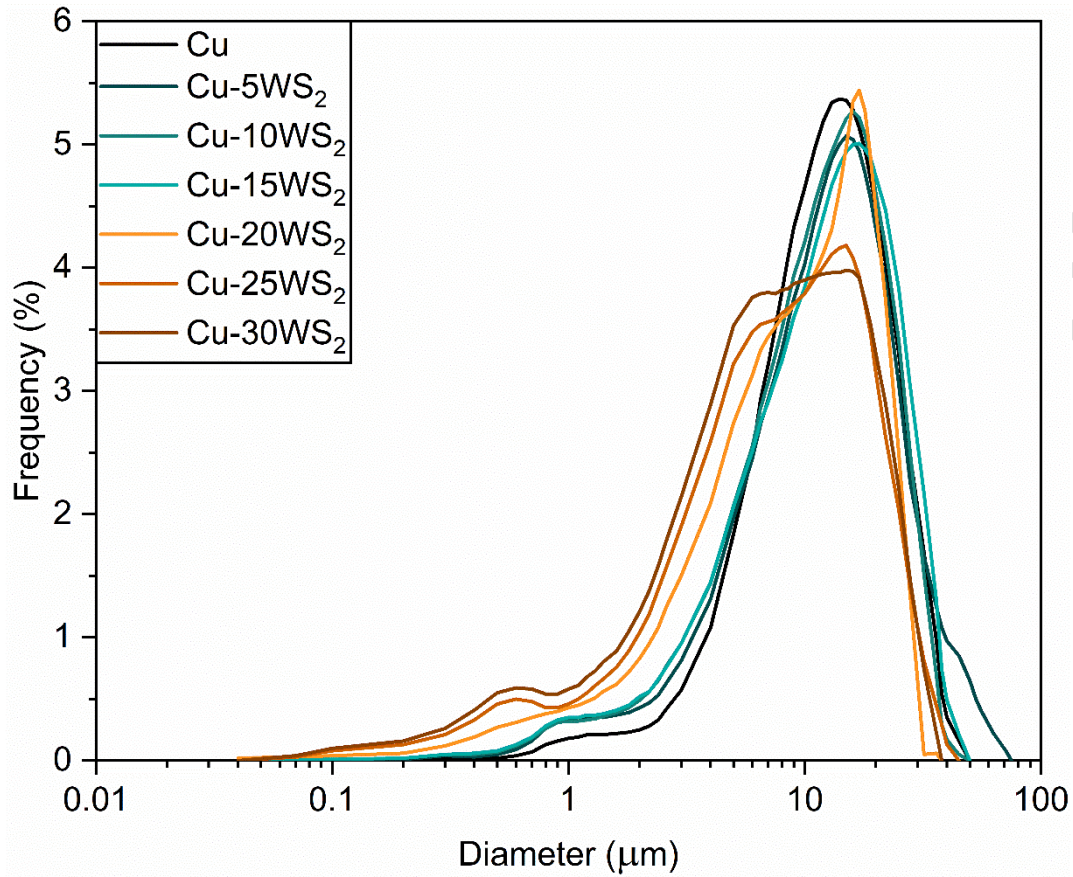


Fig. 3 Particle size distributions of reference Cu and of the Cu-XWS₂ composites.

3.2 X-ray diffraction

X-ray diffraction (XRD) patterns of the Cu-XWS₂ composites are highlighted in Fig. 4. Typical copper peaks can be noticed at about 43° for Cu (1 1 1), at about 51° for Cu (2 0 0) and at about 74° for Cu (2 2 0) [18,20,36–39]. Tungsten disulfide peaks are detected at about 14° for WS₂ (0 0 2), near to 29° for WS₂ (0 0 4), at 44° for WS₂ (0 0 6) and at about 59° for WS₂ (0 0 8) [10,18,20,40,41]. The intensity of the lubricant peaks coherently raises with the increase of its concentration (Fig. 4a) and, parallel, the opposite behavior is observed for Cu peaks (Fig. 4b). No evidence of the presence of undesired phases are found, irrespective of the employed WS₂ concentration. Specifically, Cu₂S characteristic peaks in the $20\text{--}35^\circ$ range [42,43] are not detected, thus ruling out a reaction between copper and tungsten disulfide. Moreover, decomposition issues can also be ignored: tungsten typical peaks at 40° for W (1 1 0), at 57° for W (2 0 0), and at 72° for W (2 1 1) [45] are not observed.

Therefore, the discussed preparation method can be considered sufficiently reliable in terms of chemical stability of the composites.

PRE-PRINT VERSION

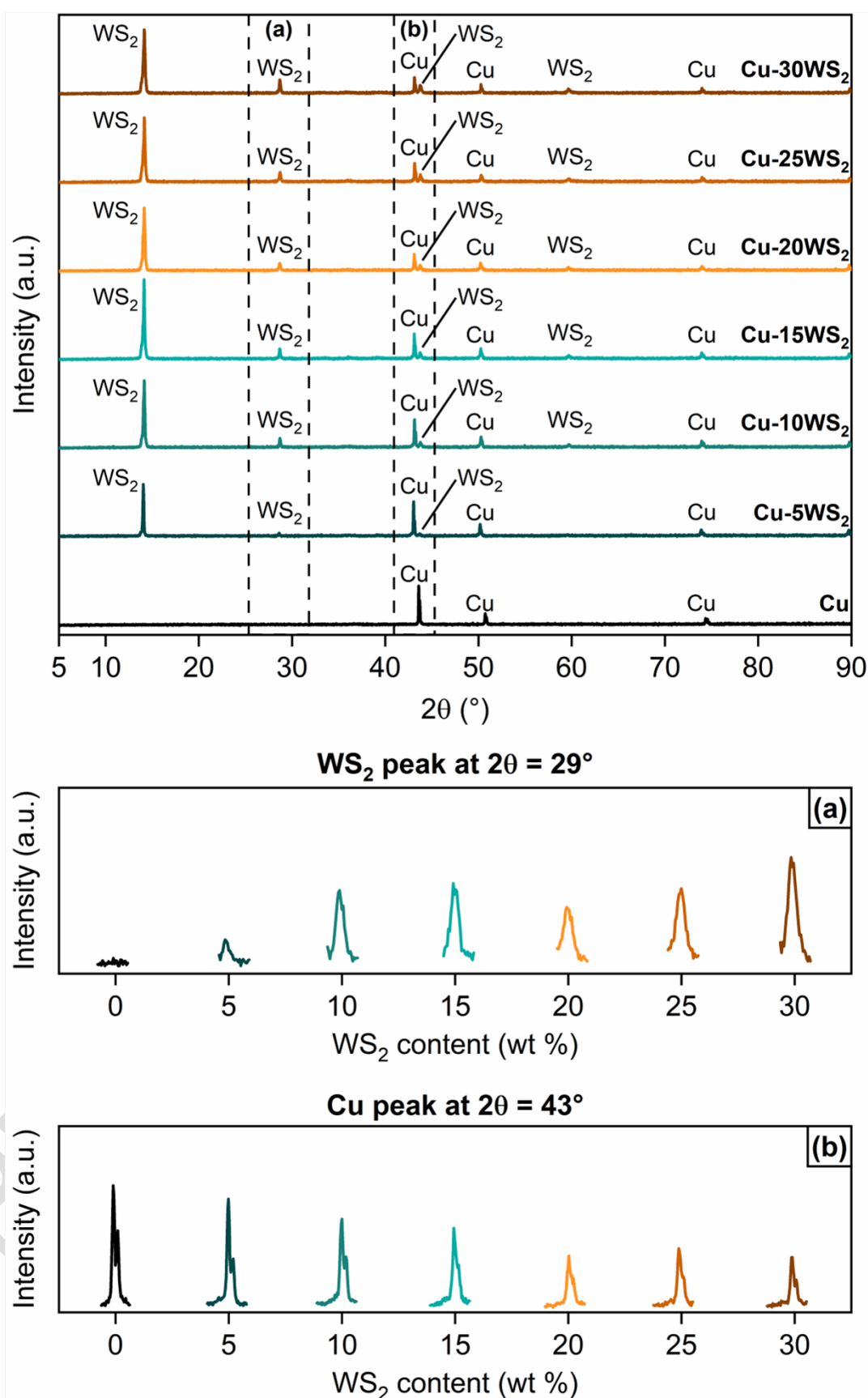


Fig. 4 XRD patterns of reference Cu and of the Cu-XWS₂ composites; (a) intensity trend of the WS₂ peak at 29° depending on WS₂ content; (b) intensity trend of the Cu peak at 43° depending on WS₂ content.

3.3 Optical contact angle

Fig. 5 portrays average static contact angle measurements taken on the Cu-XWS₂ samples, along with the corresponding standard deviations extrapolated from ten measurements. The prepared composites reveal a hydrophobic behavior, with values ranging from 108.4±6.8° of Cu-25WS₂ to 131.0±1.8° of Cu-5WS₂. This last value slightly exceeds the one measured for benchmark Cu-10WS₂ (130.0±3.4° [26]). Except for Cu-25WS₂, the combination of the copper matrix with tungsten disulfide tends to accentuate the hydrophobicity of pure copper, previously investigated by our research group (OCA of 116.4±5.2° [26]). However, the addition of larger contents of tungsten disulfide reduces the static contact angle values, hence slightly enhancing the wettability of the composites, likely due to the hydrophilicity of virgin WS₂ powders [41]. Considering a potential application of copper-based composites in sliding electrical contacts working under harsh conditions, i.e., in the aerospace sector, a high hydrophobicity would be required to strongly limit the undesired formation of a uniform ice layer at high altitudes and low temperatures.

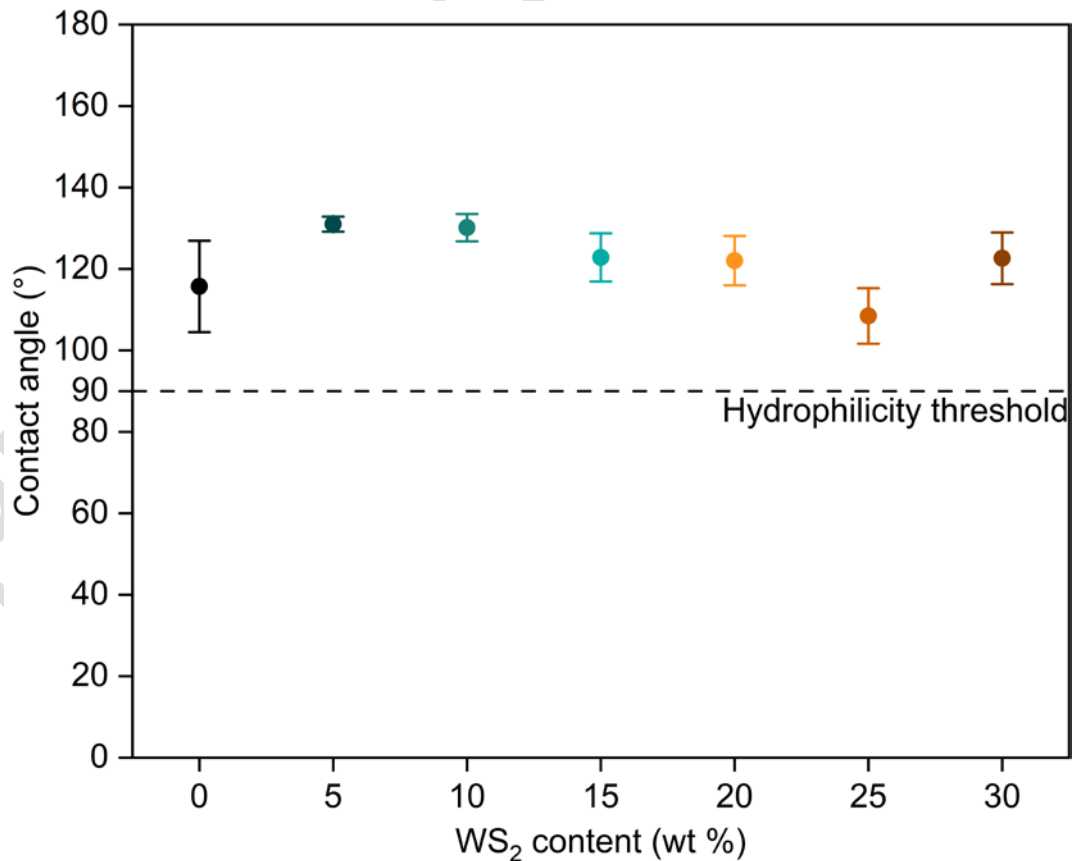


Fig. 5 Optical contact angle results of reference Cu and of the Cu-XWS₂ composites.

3.4 Scanning electron microscopy

SEM images of the cross-sections of Cu-10WS₂ and Cu-30WS₂ are collected in Fig. 6, to better appreciate the change in microstructure due to different WS₂ concentrations. The brighter phase has been identified as the solid lubricant, whereas the grey one is the copper matrix [25]. WS₂ particles appear homogeneously distributed within benchmark Cu-10WS₂ (Fig. 6(a1)-6(a3)) and mainly arranged in elongated clusters, whose presence visibly grows with the increase of the lubricating agent content up to 30 wt %. This homogeneity could be favorable from the standpoint of the composites frictional behavior, as reported in other works [46]. The black spots dispersed in the microstructure could be attributed to micro-porosity [18] resulting from a very localized interfacial debonding. It can be noticed that the spots are larger and more visible in Cu-30WS₂ (Fig. 6(b1)-6(b3)), for which a lower relative density is expected. The absence of darker zones associated to Cu₂S at the WS₂-Cu interface confirms a correct execution of the proposed preparation method, which permits to avoid undesired chemical reactions and, consequently, the preservation of the existing phases in the final composites as already deduced from X-ray diffraction outcomes (Section 3.2).

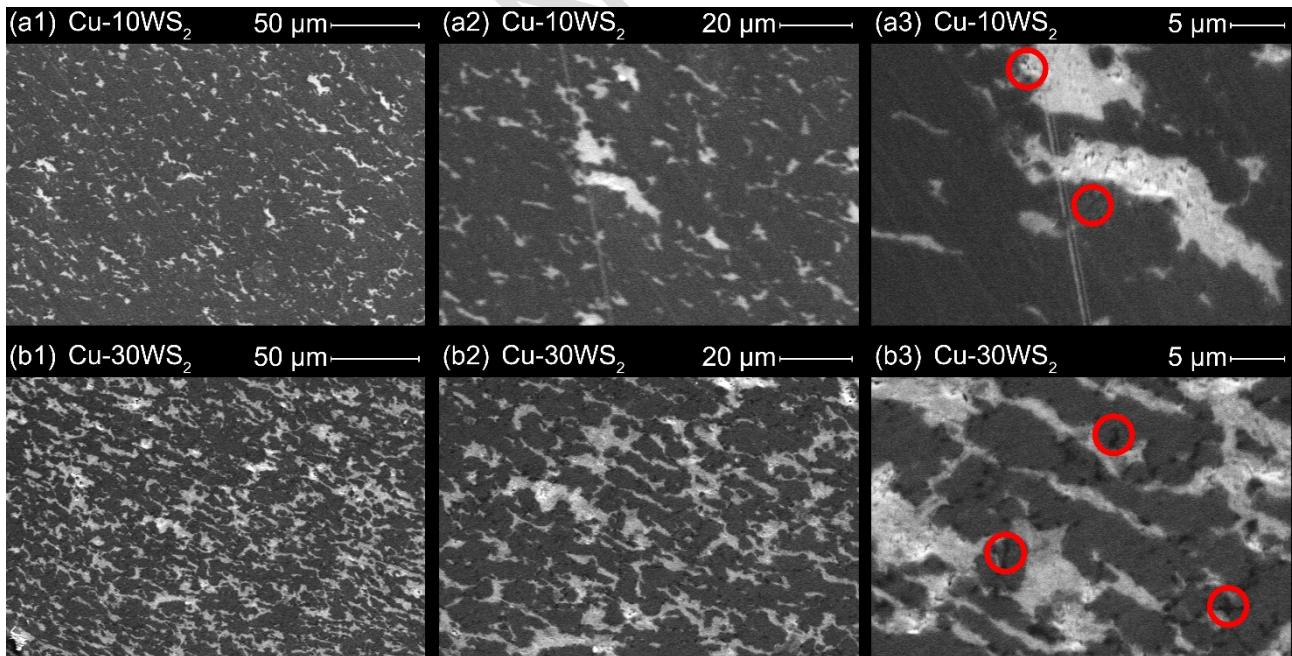


Fig. 6 SEM images of the cross-section of Cu-XWS₂ composites: Cu-10WS₂ at 500x (a1), 1000x (a2), and 3000x (a3), Cu-30WS₂ at 500x (b1), 1000x (b2), and 3000x (b3).

3.5 Density

Absolute and relative densities of the Cu-XWS₂ composites are summarized in Table 1, whereas relative density values are highlighted as a function of WS₂ content in Fig. 7. In general, the addition of WS₂ causes a slight decrease in density of the produced tablets, as expected considering the lower density of the second phase (7.50 g cm⁻³ [47]) with respect to pure copper (7.69±0.01 g cm⁻³). Consequently, it can be hypothesized that low lubricant concentrations could contribute to optimize the compaction of the final product. Nevertheless, a residual internal porosity can be recognized for all the composites, as observed from SEM images; it could be likely related to the lower efficiency in filling voids of the cold-pressing and hot-sintering process with respect to those relying on hot-pressing, and probably to the short employed sintering time.

Table 1. Absolute and relative densities of reference Cu and of the Cu-XWS₂ composites.

Sample	Absolute density (g cm ⁻³)	Relative density (%)
Cu	7.69 ± 0.01	85.83 ± 0.09
Cu-5WS ₂	7.67 ± 0.01	85.62 ± 0.11
Cu-10WS ₂	7.65 ± 0.01	85.36 ± 0.09
Cu-15WS ₂	7.54 ± 0.02	84.19 ± 0.20
Cu-20WS ₂	7.53 ± 0.01	83.99 ± 0.07
Cu-25WS ₂	7.43 ± 0.01	82.94 ± 0.10
Cu-30WS ₂	7.36 ± 0.01	82.17 ± 0.09

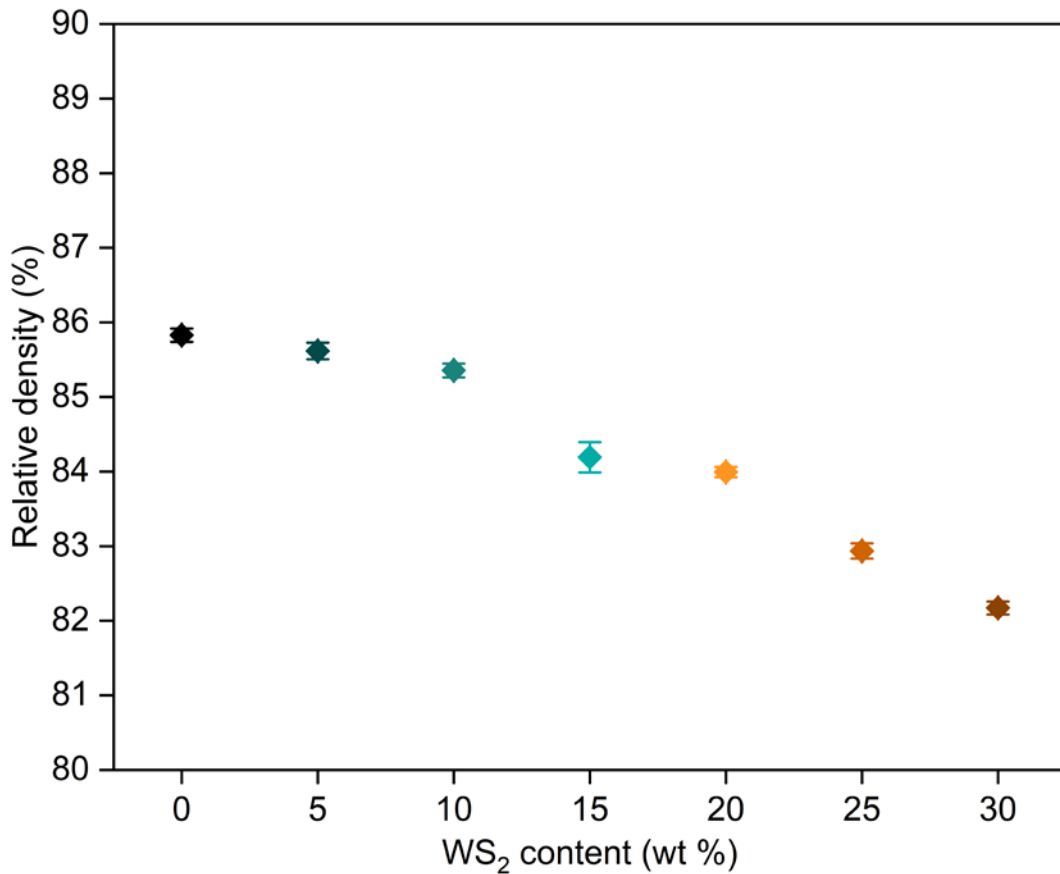


Fig. 7 Relative density values of reference Cu and of the Cu-XWS₂ composites.

3.6 Electrical resistivity

Electrical resistivity measurements of the Cu-XWS₂ samples are reported in Fig. 8. The resistivity of the fabricated composites increases with raising lubricant content and composite porosity. This behavior is coherent considering the semiconducting nature of layered TMDs such as tungsten disulfide [48]. However, a too high resistivity is undesired in sliding electrical contacts, due to the necessity of ensuring an adequate current flow. Sensitivity to WS₂ content is contained up to 20 wt %, as the samples demonstrate acceptable resistivity values in the same order of magnitude of the employed copper powder [26], which is slightly less conductive than pure copper ($1.68 \times 10^{-8} \Omega \text{ m}$ [49]) due to porosity and oxidation issues [50]. On the contrary, a steep growth towards one order of magnitude higher-values is observed for Cu-25WS₂ and Cu-30WS₂. In these cases, the second phase negatively influences the electrical properties of the composites up to unsatisfactory values.

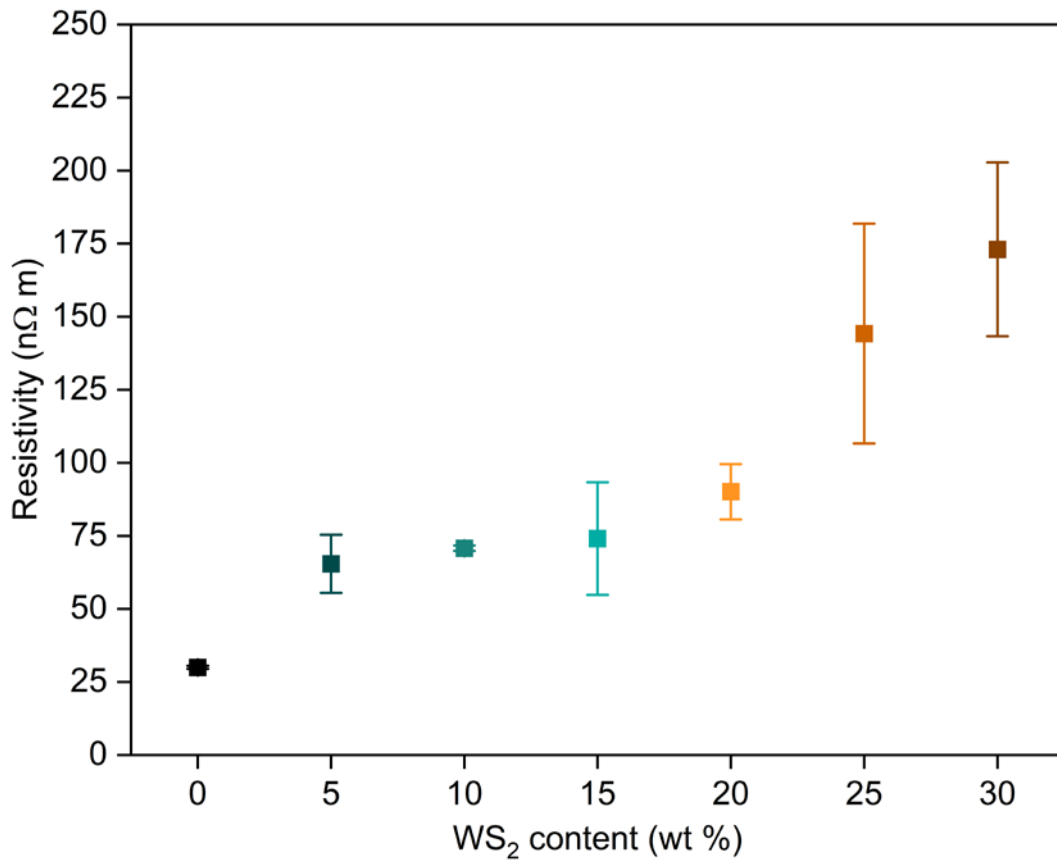


Fig. 8 Electrical resistivity values of reference Cu and of the Cu-XWS₂ composites.

3.7 Scratch test results

Fig. 9 depicts apparent friction coefficient and scratch hardness results of the Cu-XWS₂ samples. The lubricating ability of tungsten disulfide can be recognized by the slight reduction in friction coefficient exhibited by Cu-5WS₂ with respect to pure copper powder [26]. A slightly decreasing trend of FC with increasing lubricant concentration is apparent up to 20 wt % content, although for higher values of concentration data scatter becomes significantly larger, probably due to material inhomogeneity at the small scale probed by micro-scratch testing (Fig. 9(a)). This outcome suggests that no particular advantages in terms of FC are obtained by including high quantities of tungsten disulfide.

Scratch hardness performances of the Cu-XWS₂ composites are shown in Fig. 9(b). Composites up to 15 wt % WS₂ content are harder than pure copper. Conversely, larger concentrations of solid

lubricant (20, 25, 30 wt %) result in a softer material, thanks to an evident decreasing trend of hardness with increasing content of WS₂.

Overall, scratch data would suggest that benchmark Cu-10WS₂ has the highest potential of succeeding when used for sliding electrical contacts working under harsh conditions: it combines a reduction of friction common to all composites with the highest hardness value.

Another desired feature offered by composites containing up to 10 wt % of WS₂ is shown by optical microscopy images of the scratch grooves, Fig. 10: there is no significant debris formation detected, something which is very important in view of applications like slip rings. Increasing the content of second phase, the amount of debris generated during scratch testing considerably rises, with the material becoming more brittle and prone to edge cracking phenomena. Considering the dangerousness of an excessive presence of debris in terms of generation of electrical arches and damages on sliding components, a WS₂ concentration larger than 10 wt % would result inappropriate. SEM images at different magnifications of the scratch groove on Cu-5WS₂ are shown in Fig. 11. It is possible to notice several agglomerates of solid lubricant as white spots spread out on the groove (Fig. 11(b)-11(c)); hence an effective lubricating action could not be presumed. Specific wear rates and wear coefficients, depicted in Fig. 12, have been calculated from the experimental data as explained in Section 2.11. The values trend is consistent with the computed scratch hardness: Cu-10WS₂, which has the highest hardness outcome (787.9 ± 66.6 MPa), coherently exhibits the lowest specific wear rate ($1.14 \pm 0.08 \times 10^{-1} \text{ mm}^3 \text{ N}^{-1} \text{ m}^{-1}$) and wear coefficient ($8.96 \pm 0.64 \times 10^{-2}$). Therefore, it can be stated that a single pass test emphasizes the softening effect caused by higher solid lubricant concentrations on the composites, since the formation of a uniform tribo-film is not expected. Wear coefficient values corroborate this observation, as their order of magnitude (10^{-1} – 10^{-2}) falls within the “wear by hard particles” regime [51] independently from the WS₂ content, even though friction coefficients are acceptable.

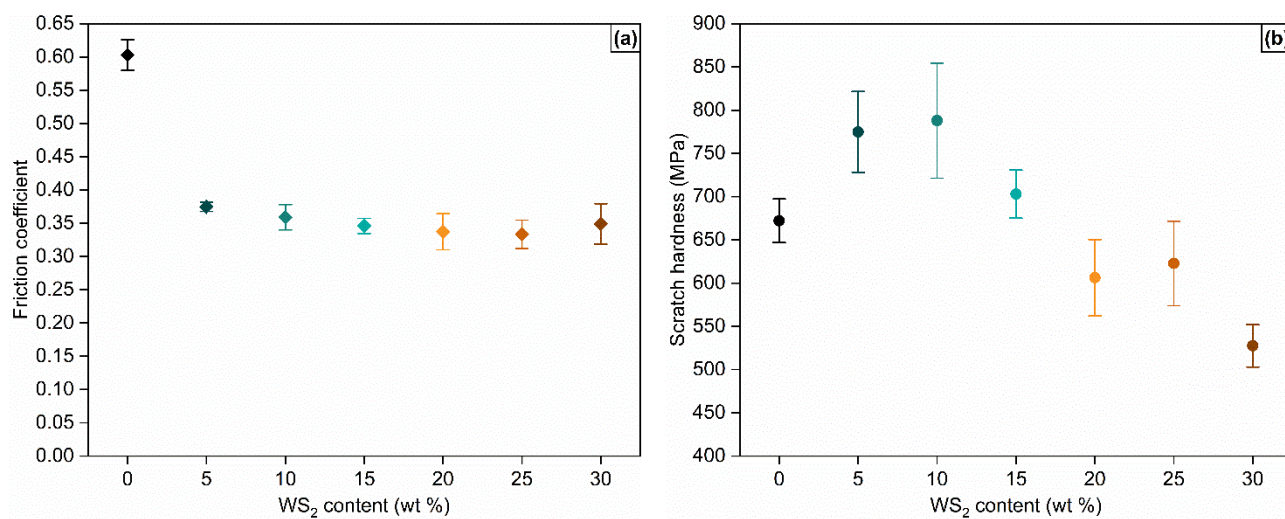


Fig. 9 (a) Friction coefficients and (b) scratch hardness values of reference Cu and of the Cu-XWS₂ composites.

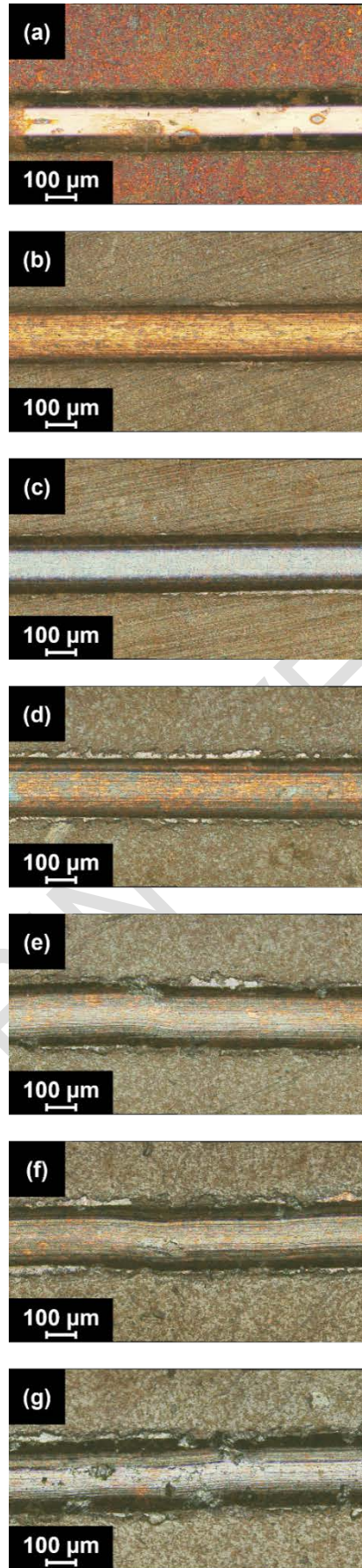


Fig. 10 OM images of the scratches of (a) reference Cu and of the Cu-XWS₂ composites at 20x magnification: (b) Cu-5WS₂, (c) Cu-10WS₂, (d) Cu-15WS₂, (e) Cu-20WS₂, (f) Cu-25WS₂, (g) Cu-30WS₂.

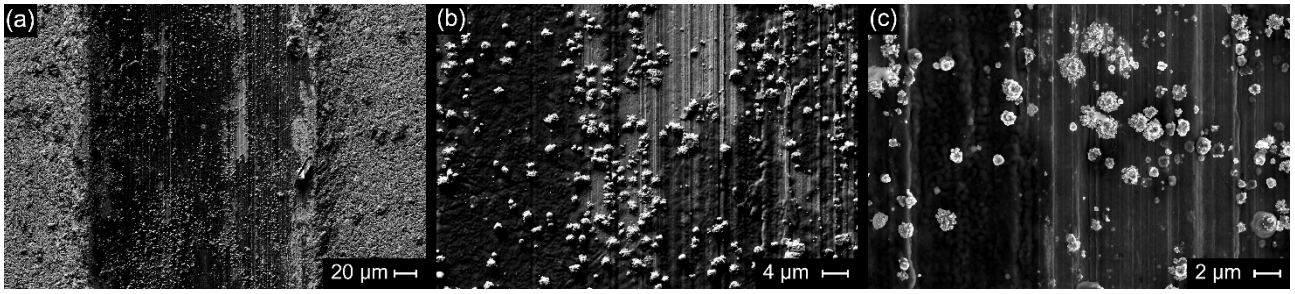


Fig. 11 SEM images of the scratches of Cu-5WS₂ at different magnifications: (a) 800x, (b) 5000x, (c) 10000x.

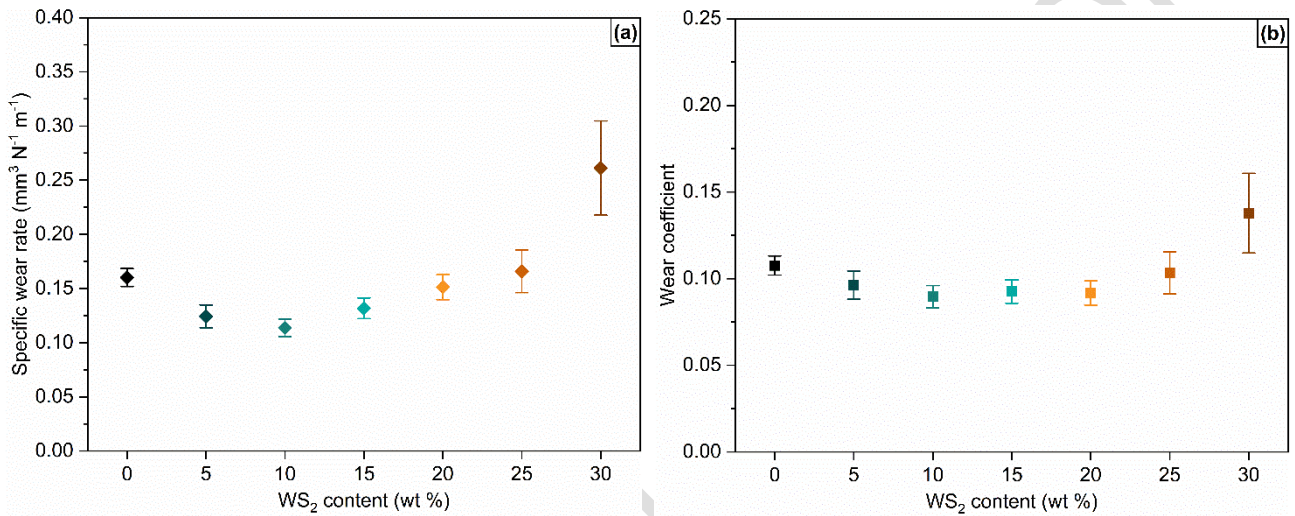


Fig. 12 (a) Specific wear rates and (b) wear coefficients of reference Cu and of the Cu-XWS₂ composites extrapolated from scratch tests.

3.8 Vickers hardness

Vickers hardness values of the Cu-XWS₂ composites, reported in Fig. 13, appear to be consistent with scratch hardness ones, as expected [29,30]. The effect of tungsten disulfide on the Vickers hardness of copper-based composites differs from the one of other solid lubricants, such as carbonaceous phases. Previous studies have proved an overall hardness decrease provoked by the combination of a copper matrix with species of soft nature, such as graphite [23,24,51,52]. Conversely, WS₂ contributes to the strengthening of the manufactured samples with respect to virgin copper. As it can be noticed, a second phase concentration of 5 wt % leads to a Vickers hardness value of 67.5 ± 1.2 HV. A further growth up to 71.0 ± 1.5 HV is witnessed for benchmark Cu-10WS₂, then hardness performances tend to progressively decrease. This behavior is coherent with results

obtained by other authors [18,53]. This behavior could be explained by an active synergy between Cu and WS₂, promoted by the anisotropic lamellar structure of the TMD and its strong interfacial bonding with the metal matrix [19]. This beneficial effect is exerted up to a threshold amount of lubricant, which can be identified at about 10 wt %. Once this boundary is overcome, the probable redistribution of anisotropic WS₂ particles, visible in the particle size curves (Fig. 3) as a frequency peak at low diameter size ($\approx 0.6 \mu\text{m}$), hinders the beneficial impact on the mechanical properties of the composite, in particular on both scratch and indentation hardness.

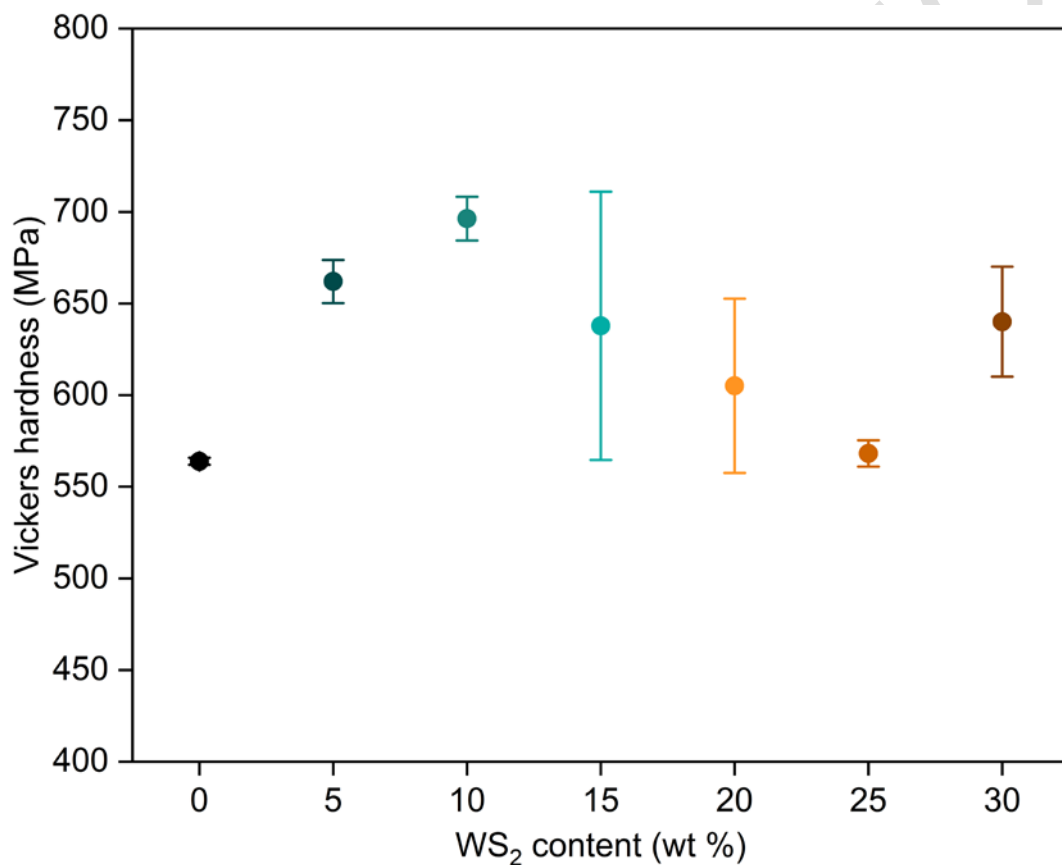


Fig. 13 Vickers hardness values of reference Cu and of the Cu-XWS₂ composites.

3.9 Wear test results

Fig. 14 illustrates the friction coefficients of Cu-XWS₂ samples as a function of the distance covered during wear tests (500 m). The lubricating effect of tungsten disulfide is evident, as friction coefficients values of the Cu-XWS₂ composites are significantly lower than 0.75, previously measured by our research group for a pure electrolytic copper tablet [26] and consistent with literature

values [19]. The initial higher outcomes, exhibited by all the analyzed composites, could be attributed to a running stage in which the coupling between the counter ball and the Cu-XWS₂ disks is not completed. Once the actual mating is accomplished after a sliding distance of roughly 150 m, a reduction of friction coefficient is found and then a steady state condition is maintained, with values general ranging from 0.12 and 0.18. As already discussed, the lubricating capability of WS₂ derives from its sandwich-like crystal structure. The dangling and unsaturated bonds on the edge of the WS₂ basal planes are prone to react with environmental moisture and oxygen to form tribo-oxidation products, such as WO₃. As a consequence, the developed lubricating layers can easily slide under shearing stress. The movement of the ball on the tablets surface is therefore facilitated [16,18].

Fig. 15 shows OM images of the wear tracks generated on the Cu-XWS₂ composites. At first sight, the increasing content of second phase can be appreciated through the color change of the contact area from a typical copper shade (Cu-5WS₂) to a light blue-gray one (Cu-30WS₂). A non-homogeneous appearance of all wear scars can be witnessed, similarly to benchmark Cu-10WS₂ [26]. It could be attributed to a chipping phenomenon caused by the sliding of the counter ball. Therefore, an abrasive wear mechanism can be hypothesized at low WS₂ content. The track width of Cu-5WS₂ (1309 μm) is comparable to benchmark Cu-10WS₂ (1255 μm) due to the higher hardness of these samples, which provokes a broadening of the counter ball contact zone. Cu-20WS₂ and Cu-30WS₂ display wear tracks with variable width (716–1032 μm and 726–876 μm , respectively). A possible explanation is the formation of surface asperities that act as third bodies, progressively hindering the correct contact between the surfaces and outrunning them. The effective action of the solid lubricant can be observed at higher content, with Cu-25WS₂ exhibiting the smoother wear track with almost constant width (843 μm). The homogeneity of the contact area could be associated to the ability of WS₂ in promoting an adhesive wear mechanism, preventing a direct metal-to-metal interaction via the formation of a lubricating film that becomes more continuous at increased WS₂ concentration [19].

SEM morphologies of post-wear test samples are gathered in Fig. 16. Specifically, Cu-5WS₂, Cu-15WS₂, and Cu-30WS₂ have been chosen as lower limit, middle value, and upper limit of second phase concentration to facilitate the comprehension of how WS₂ impacts on the wear behavior of the composites. The uneven aspect of Cu-5WS₂ wear track (Fig. 16(a1)) is confirmed by SEM analysis. Micro-cracks and pile-up of removed material are the consequence of an overall abrasive mechanism, due to which the sample is plastically deformed. The progressive increase of second phase content guarantees a transition towards the formation of a more uniform tribo-layer, by which WS₂ exerts its lubricating effect [18]. An adhesive mechanism may be therefore triggered and WS₂ sheets released on the surface, limiting the contact between the composites and the counterpart [25]. SEM image at 400x of Cu-30WS₂ (Fig. 16(c1)) is obtained in a narrowing zone, hence track borders are visible. As previously asserted, this periodic width variation may be related to the presence of third bodies that complicate the sliding of the counter ball and cause the generation of rough-edged debris (Fig. 16(c2)). Cross-sectional images perpendicular to the sliding direction allow to observe the profile of stratified material due to detachment and reattachment forced by the counter ball movement.

Fig. 17 shows specific wear rates and wear coefficients of the Cu-XWS₂ composites, computed as described in Section 2.11 by exploiting the profiles as exemplified in Fig. 2. The results demonstrate a decrease in wear coefficient (Fig. 17(b)) as the second phase content increases. The best performance is exhibited by the samples with the highest WS₂ concentration (Cu-25WS₂ and Cu-30WS₂), but it can be underlined that Cu-15WS₂ has a wear coefficient within the same order of magnitude (10^{-5}) of the above-mentioned composites despite a lower second phase content. The calculated wear coefficients fall within the “mild” wear regime, which is typically characterized by the formation of fine debris [51] as confirmed by OM and SEM analyses. The discrepancy between these values and the ones extrapolated from scratch tests (order of magnitude of 10^{-1} – 10^{-2}) can be mainly attributed to the experimental setup differences: the multiple-pass of the counter ball on the tested surface leads to the activation of the lubricating effect of WS₂ and, consequently, further confirms the formation of a tribo-film. The positive aspect of the discussed outputs is that a wear test

better approximates the actual operating conditions of a sliding electrical contact, therefore the performance of the prepared composites can be considered adequate.

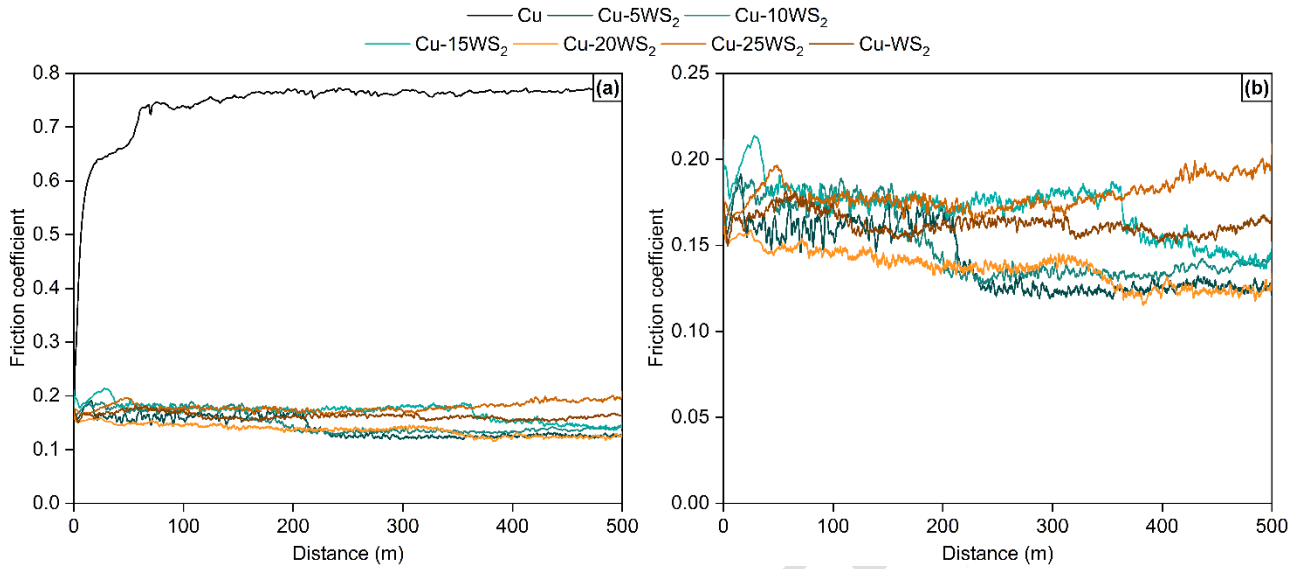


Fig. 14 (a) Friction coefficient trends of reference Cu and of the Cu-XWS₂ composites from wear tests; (b) details on the friction coefficients of the Cu-XWS₂ composites.

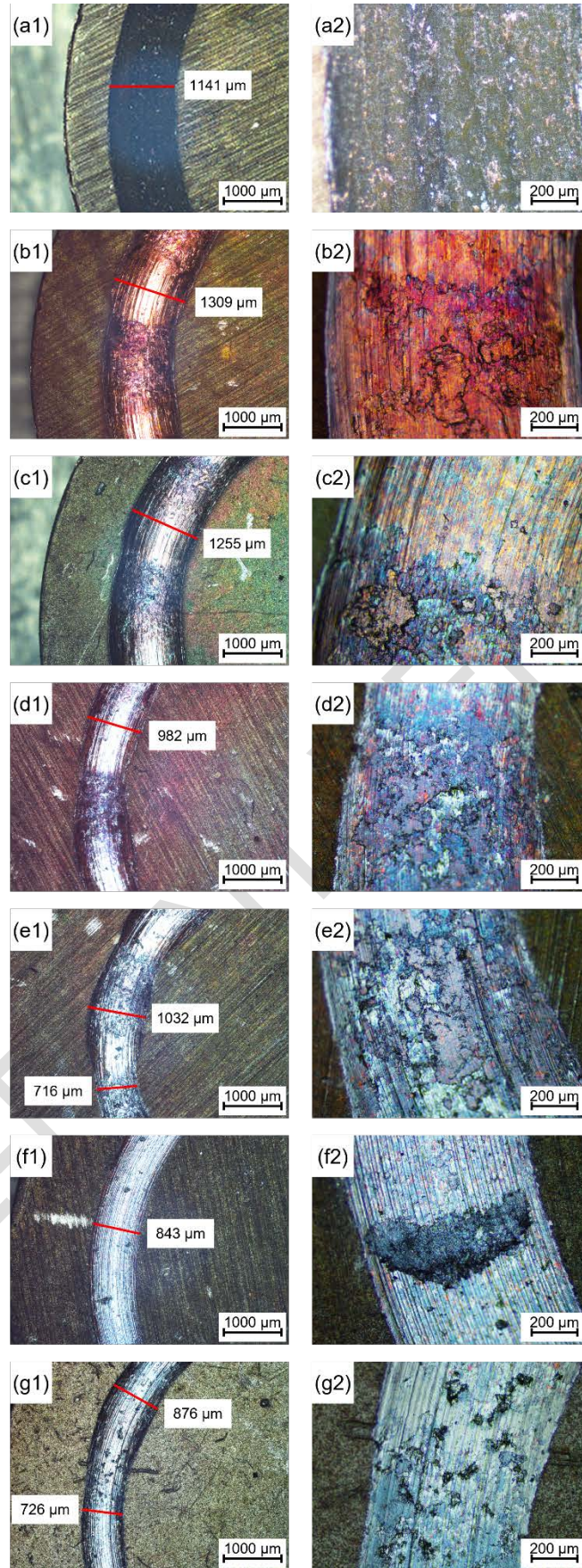


Fig. 15 OM images of the wear tracks of reference Cu and of the Cu-XWS₂ composites: Cu at 25x (a1) and 50x (a2), Cu-5WS₂ at 25x (b1) and 50x (b2), Cu-10WS₂ at 25x (c1) and 50x (c2), Cu-15WS₂ at 25x (d1) and 50x (d2), Cu-20WS₂ at 25x (e1) and 50x (e2), Cu-25WS₂ at 25x (f1) and 50x (f2), Cu-30WS₂ at 25x (g1) and 50x (g2).

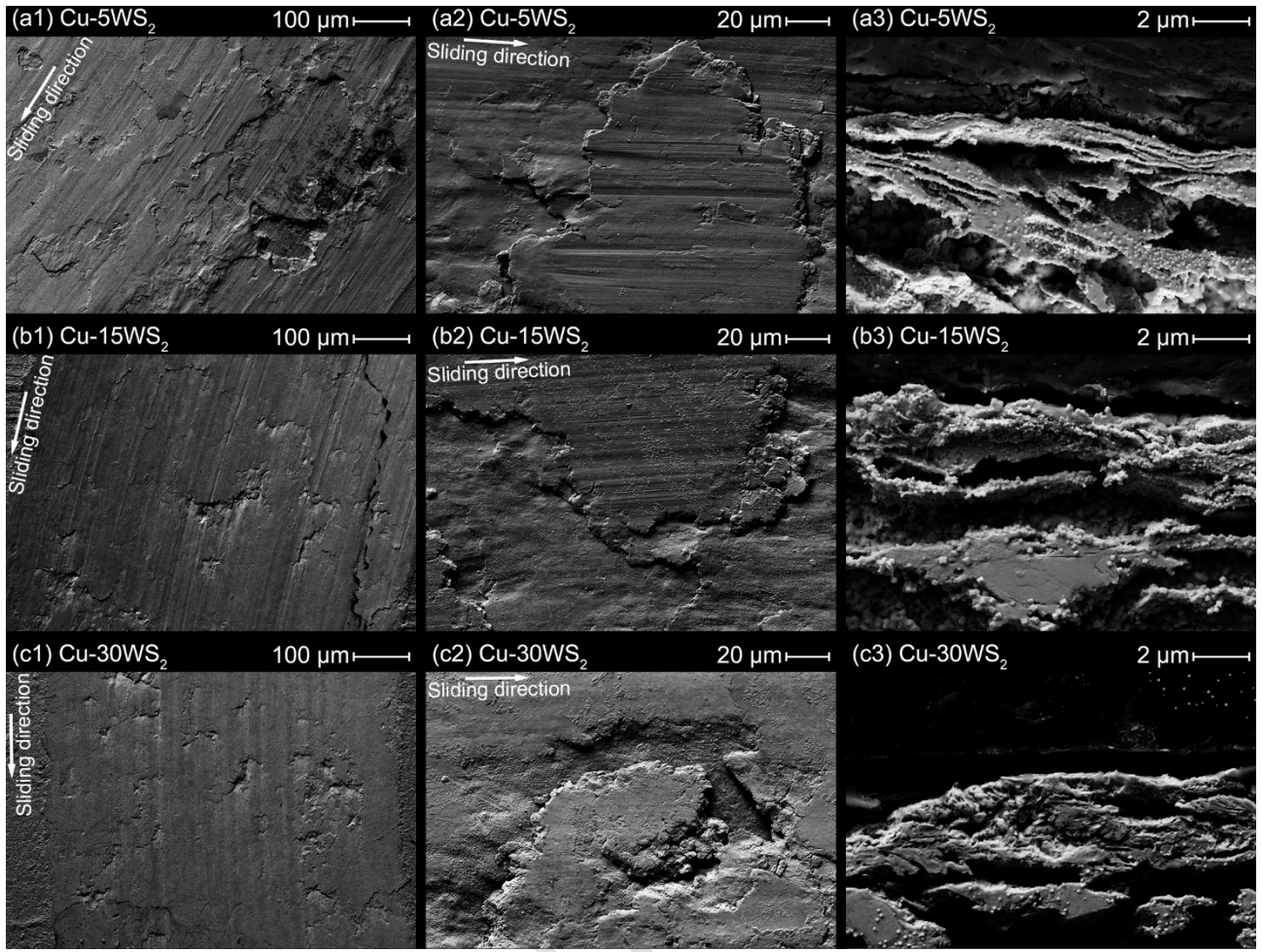


Fig. 16 SEM images of the wear tracks of Cu-XWS₂ composites: Cu-5WS₂ at 400x (a1), 1500x (a2) and cross-section at 20000x (a3), Cu-15WS₂ at 400x (b1), 1500x (b2) and cross-section at 20000x (b3), Cu-30WS₂ at 400x (c1), 1500x (c2) and cross-section at 20000x (c3).

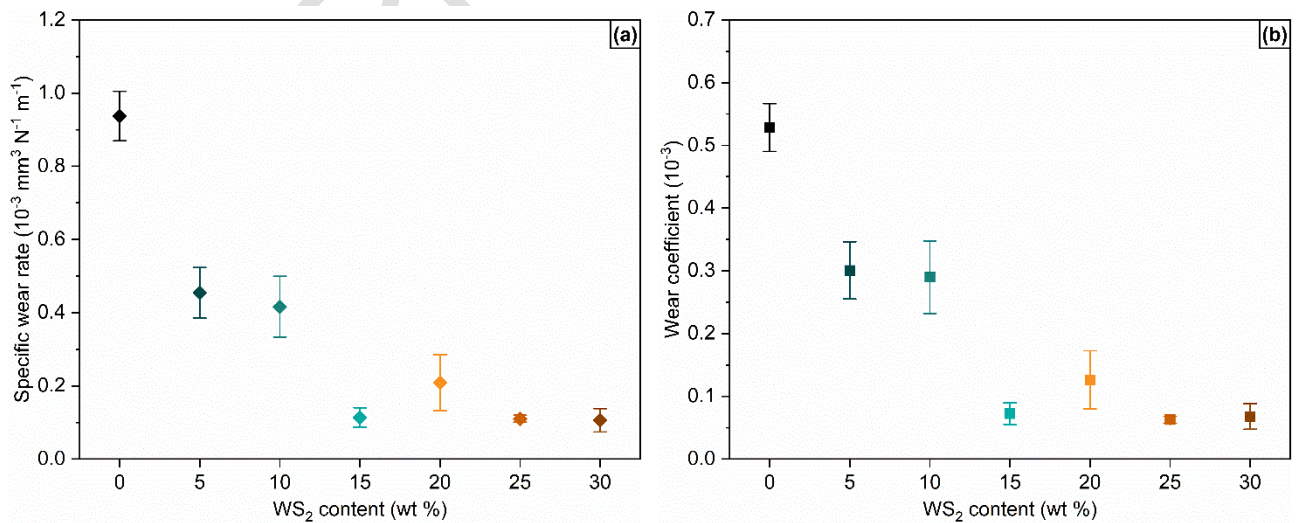


Fig. 17 (a) Specific wear rates and (b) wear coefficients of reference Cu and of the Cu-XWS₂ composites extrapolated from wear tests.

4. Conclusions

The present study reports an investigation about the effects of second phase content between 5 and 30 wt % on the tribological, mechanical, electrical and wettability properties of self-lubricating Cu-WS₂ composites for a potential application in sliding electrical contacts working under harsh conditions. The samples have been manufactured via a powder metallurgy process, consisting of a ball milling step, a cold-pressing and a pressureless hot-sintering process. The experimental outcomes pointed out that WS₂ substantially improves the wettability and the wear behavior of the investigated composites with respect to pristine copper. Scratch and Vickers hardness of the samples are as well enhanced up to a 15 wt % content of second phase, while electrical conductivity is not excessively hindered. However, a filler amount larger than 20 wt % led to material softening, a one order of magnitude increase in resistivity and also a slight reduction in hydrophobicity. Considering that adequate electrical conductivity and high hydrophobicity are paramount for an application in sliding electrical contacts, the inclusion of larger contents of WS₂ in these composites is not recommended, at least for the particular application considered. From the interpretation of wear test results, an abrasive wear mechanism can be hypothesized for low WS₂ contents, whereas the solid lubricant shall promote a switch to a predominantly adhesive mechanism at high concentrations, thus ensuring a better self-lubricating behavior of the composites. Extrapolated specific wear rates and wear coefficients support this statement, since lower values are obtained once the WS₂ content exceeds 10 wt %; composites with 15 wt %, 25 wt % and 30 wt % of WS₂ provide the best wear performance. Therefore, it can be concluded that the optimal trade-off between tribological, electrical and wettability properties should be surveyed in the range of 10–15 wt % of tungsten disulfide. Further analyses are mandatory to gain a better understanding of the actual degradation mechanism of Cu-WS₂ composites.

Acknowledgements

The authors would like to thank the EIT Raw Materials that funded this work within the project ADMA 2 – Practical training between Academia and Industry during doctoral studies (Project n. 18252), and Logic S.p.A. for the supply of materials and instruments.

References

- [1] Shin WG, Lee SH. An analysis of the main factors on the wear of brushes for automotive small brush-type DC motor. *J Mech Sci Technol* 2010;24:37–41.
<https://doi.org/10.1007/s12206-009-1135-4>.
- [2] Holm R. *Electric Contacts*. Berlin, Heidelberg: Springer Berlin Heidelberg; 1967.
<https://doi.org/10.1007/978-3-662-06688-1>.
- [3] Xiao JK, Liu LM, Zhang C, Zhang L, Zhou KC. Sliding electrical contact behavior of brass fiber brush against coin-silver and Au plating. *Wear* 2016;368–369:461–9.
<https://doi.org/10.1016/j.wear.2016.10.007>.
- [4] Slade PG. *Electrical Contacts, Principles and Applications*. Second Edi. Boca Raton, FL: CRC Press - Taylor & Francis Group; 2014.
- [5] Wang QJ, Chung Y-W, editors. *Encyclopedia of Tribology*. Boston, MA: Springer US; 2013.
<https://doi.org/10.1007/978-0-387-92897-5>.
- [6] Argibay N, Sawyer WG. Low wear metal sliding electrical contacts at high current density. *Wear* 2012;274–275:229–37. <https://doi.org/10.1016/j.wear.2011.09.003>.
- [7] Bares JA, Argibay N, Dickrell PL, Bourne GR, Burris DL, Ziegert JC, et al. In situ graphite lubrication of metallic sliding electrical contacts. *Wear* 2009;267:1462–9.
<https://doi.org/10.1016/j.wear.2009.03.024>.
- [8] Furlan KP, de Mello JDB, Klein AN. Self-lubricating composites containing MoS₂: A review. *Tribol Int* 2018;120:280–98. <https://doi.org/10.1016/J.TRIBOINT.2017.12.033>.
- [9] Tyagi R, Das AK, Mandal A. Electrical discharge coating using WS₂ and Cu powder

mixture for solid lubrication and enhanced tribological performance. *Tribol Int* 2018;120:80–92. <https://doi.org/10.1016/J.TRIBOINT.2017.12.023>.

- [10] Zhu S, Cheng J, Qiao Z, Yang J. High temperature solid-lubricating materials: A review. *Tribol Int* 2019;133:206–23. <https://doi.org/10.1016/J.TRIBOINT.2018.12.037>.
- [11] Kang X, Zhang L. Enhanced sliding electrical contact properties of silver matrix self-lubricating nanocomposite using molecular level mixing process and spark plasma sintering. *Powder Technol* 2020;372:94–106. <https://doi.org/10.1016/j.powtec.2020.05.062>.
- [12] Xiao J, Wu Y, Zhang W, Chen J, Zhang C. Friction of metal-matrix self-lubricating composites: Relationships among lubricant content, lubricating film coverage, and friction coefficient. *Friction* 2020;8:517–30. <https://doi.org/10.1007/s40544-019-0270-x>.
- [13] Yuan J, Yao Y, Zhuang M, Du Y, Wang L, Yu Z. Effects of Cu and WS₂ addition on microstructural evolution and tribological properties of self-lubricating anti-wear coatings prepared by laser cladding. *Tribol Int* 2021;157:106872. <https://doi.org/10.1016/J.TRIBOINT.2021.106872>.
- [14] Grandin M, Wiklund U. Wear phenomena and tribofilm formation of copper/copper-graphite sliding electrical contact materials. *Wear* 2018;398–399:227–35. <https://doi.org/10.1016/j.wear.2017.12.012>.
- [15] Natarajan N, Krishnaraj V, Davim JP. Metal Matrix Composites - Synthesis, Wear Characteristics, Machinability Study of MMC Brake Drum. 2015.
- [16] Prasad S, McDevitt N, Zabinski J. Tribology of tungsten disulfide films in humid environments: *Wear* 1999;230:24–34. [https://doi.org/10.1016/s0043-1648\(99\)00082-4](https://doi.org/10.1016/s0043-1648(99)00082-4).
- [17] Wong KC, Lu X, Cotter J, Eadie DT, Wong PC, Mitchell KAR. Surface and friction characterization of MoS₂ and WS₂ third body thin films under simulated wheel/rail rolling-sliding contact. *Wear* 2008;264:526–34. <https://doi.org/10.1016/j.wear.2007.04.004>.
- [18] Zhao L, Yao P, Gong T, Zhou H, Deng M, Wang Z, et al. Effect of Adding Tungsten Disulfide to a Copper Matrix on the Formation of Tribo-Film and on the Tribological

Behavior of Copper/Tungsten Disulfide Composites. *Tribol Lett* 2019;67:1–13.

<https://doi.org/10.1007/s11249-019-1200-9>.

- [19] Xiao JK, Zhang W, Zhang C. Microstructure evolution and tribological performance of Cu-WS₂ self-lubricating composites. *Wear* 2018;412–413:109–19.
<https://doi.org/10.1016/j.wear.2018.07.024>.
- [20] Zhou J, Ma C, Kang X, Zhang L, Liu X. Effect of WS₂ particle size on mechanical properties and tribological behaviors of Cu-WS₂ composites sintered by SPS. *Trans Nonferrous Met Soc China* 2018;28:1176–85. [https://doi.org/10.1016/S1003-6326\(18\)64755-7](https://doi.org/10.1016/S1003-6326(18)64755-7).
- [21] Nian J, Chen L, Guo Z, Liu W. Computational investigation of the lubrication behaviors of dioxides and disulfides of molybdenum and tungsten in vacuum. *Friction* 2017;5:23–31.
<https://doi.org/10.1007/s40544-016-0128-4>.
- [22] Srivastava SK, Avasthi BN. Layer type tungsten dichalcogenide compounds: their preparation, structure, properties and uses. *J Mater Sci* 1985;20:3801–15.
<https://doi.org/10.1007/BF00552369>.
- [23] Brainard JA. The thermal stability and friction of the disulfides, diselenides, and ditellurides of molybdenum and tungsten in vacuum (10^{-9} to 10^{-6} TORR). 1969.
- [24] Xiao JK, Zhang L, Zhou KC, Wang XP. Microscratch behavior of copper-graphite composites. *Tribol Int* 2013;57:38–45. <https://doi.org/10.1016/j.triboint.2012.07.004>.
- [25] Wang Q, Chen M, Shan Z, Sui C, Zhang L, Zhu S, et al. Comparative study of mechanical and wear behavior of Cu/WS₂ composites fabricated by spark plasma sintering and hot pressing. *J Mater Sci Technol* 2017;33:1416–23. <https://doi.org/10.1016/j.jmst.2017.06.014>.
- [26] Freschi M, Di Virgilio M, Zanardi G, Mariani M, Lecis N, Dotelli G. Employment of micro- and Nano-WS₂ structures to enhance the tribological properties of copper matrix composites. *Lubricants* 2021;9. <https://doi.org/10.3390/lubricants9050053>.
- [27] Lide DR, Data SR, Board EA, Baysinger G, Chemistry S, Library CE, et al. Section 4 -

Properties of the Elements and Inorganic Compounds. CRC Handb. Chem. Phys., CRC Press; 2020, p. 722–875. <https://doi.org/10.1201/b17118-9>.

- [28] Bowden FP, Tabor D. The Friction and Lubrication of Solids. Oxford: Clarendon Press, 1964; 1964.
- [29] Briscoe BJ, Evans PD, Biswas SK, Sinha SK. The hardnesses of poly(methylmethacrylate). Tribol Int 1996;29:93–104. [https://doi.org/10.1016/0301-679X\(95\)00045-6](https://doi.org/10.1016/0301-679X(95)00045-6).
- [30] Kurkcu P, Andena L, Pavan A. An experimental investigation of the scratch behaviour of polymers: 1. Influence of rate-dependent bulk mechanical properties. Wear 2012;290–291:86–93. <https://doi.org/10.1016/j.wear.2012.05.005>.
- [31] Kurkcu P, Andena L, Pavan A. An experimental investigation of the scratch behaviour of polymers: 2. Influence of hard or soft fillers. Wear 2014;317:277–90. <https://doi.org/10.1016/j.wear.2014.03.011>.
- [32] Zum Gahr KH. Chapter 5 Grooving Wear. Tribol. Ser., vol. 10, 1987, p. 132–350. [https://doi.org/10.1016/S0167-8922\(08\)70723-5](https://doi.org/10.1016/S0167-8922(08)70723-5).
- [33] Archard JF. Contact and Rubbing of Flat Surfaces. J Appl Phys 1953;24:981–8. <https://doi.org/10.1063/1.1721448>.
- [34] Archard JF, Hirst W. The wear of metals under unlubricated conditions. Proc R Soc London Ser A Math Phys Sci 1956;236:397–410. <https://doi.org/10.1098/rspa.1956.0144>.
- [35] Huang J, Zhang Y, Wang D, Ren B, Song P, Zhang G, et al. Effect of ball milling process on the mechanical and thermal properties of the nanodiamond/2024Al composites. Micron 2021;148:103104. <https://doi.org/10.1016/j.micron.2021.103104>.
- [36] Balasubramanian P, Battabyal M, Chandra Bose A, Gopalan R. Effect of ball-milling on the phase formation and enhanced thermoelectric properties in zinc antimonides. Mater Sci Eng B Solid-State Mater Adv Technol 2021;271:115274. <https://doi.org/10.1016/j.mseb.2021.115274>.
- [37] Theivasanthi T, Alagar M. X-Ray Diffraction Studies of Copper Nanopowder. Sch Res Libr

2010;2:373–83.

- [38] Cartigueyen S, Mahadevan K. Wear characteristics of copper-based surface-level microcomposites and nanocomposites prepared by friction stir processing. *Friction* 2016;4:39–49. <https://doi.org/10.1007/s40544-016-0102-1>.
- [39] Cheng J, Mao M, Gan X, Lei Q, Li Z, Zhou K. Microstructures, mechanical properties, and grease-lubricated sliding wear behavior of Cu-15Ni-8Sn-0.8Nb alloy with high strength and toughness. *Friction* 2021;9:1061–76. <https://doi.org/10.1007/s40544-020-0399-7>.
- [40] Khan A, Rashid A, Younas R, Chong R. A chemical reduction approach to the synthesis of copper nanoparticles. *Int Nano Lett* 2016;6:21–6. <https://doi.org/10.1007/s40089-015-0163-6>.
- [41] Rodrigues SP, Polcar T, Carvalho S, Cavaleiro A. The wettability and tribological behaviour of thin F-doped WS₂ films deposited by magnetron sputtering. *Surf Coatings Technol* 2019;378:125033. <https://doi.org/10.1016/j.surfcoat.2019.125033>.
- [42] Kang X, Yu S, Yang H, Sun Y, Zhang L. Tribological behavior and microstructural evolution of lubricating film of silver matrix self-lubricating nanocomposite. *Friction* 2021;9:941–51. <https://doi.org/10.1007/s40544-020-0379-y>.
- [43] Pathan HM, Desai JD, Lokhande CD. Modified chemical deposition and physico-chemical properties of copper sulphide (Cu₂S) thin films. *Appl Surf Sci* 2002;202:47–56. [https://doi.org/10.1016/S0169-4332\(02\)00843-7](https://doi.org/10.1016/S0169-4332(02)00843-7).
- [44] Saadeldin M, Soliman HS, Ali HAM, Sawaby K. Optical and electrical characterizations of nanoparticle Cu₂S thin films. *Chinese Phys B* 2014;23. <https://doi.org/10.1088/1674-1056/23/4/046803>.
- [45] Xiong L, He T. Synthesis and characterization of ultrafine tungsten and tungsten oxide nanoparticles by a reverse microemulsion-mediated method. *Chem Mater* 2006;18:2211–8. <https://doi.org/10.1021/cm052320t>.
- [46] Rajkumar K, Aravindan S. Tribological studies on microwave sintered copper-carbon

nanotube composites. *Wear* 2011;270:613–21. <https://doi.org/10.1016/j.wear.2011.01.017>.

- [47] Sigma-Aldrich. Tungsten Disulfide Safesheet 2020:1–8.
- [48] Sik Hwang W, Remskar M, Yan R, Protasenko V, Tahy K, Doo Chae S, et al. Transistors with chemically synthesized layered semiconductor WS₂ exhibiting 10⁵ room temperature modulation and ambipolar behavior. *Appl Phys Lett* 2012;101. <https://doi.org/10.1063/1.4732522>.
- [49] Lide DR, Data SR, Board EA, Baysinger G, Chemistry S, Library CE, et al. Section 12 - Properties of Solids. *CRC Handb. Chem. Phys.*, CRC Press; 2020, p. 2085–322. <https://doi.org/10.1201/b17118-17>.
- [50] Gelbstein Y, Haim Y, Kalabukhov S, Kasiyan V, Hartmann S, Rothe S, et al. Correlation between Thermal and Electrical Properties of Spark Plasma Sintered (SPS) Porous Copper. *Sinter. Tech. Mater.*, InTech; 2015. <https://doi.org/10.5772/59010>.
- [51] Springer handbook of materials measurement methods. *Mater Today* 2006;9:52. [https://doi.org/10.1016/S1369-7021\(06\)71582-6](https://doi.org/10.1016/S1369-7021(06)71582-6).
- [52] Futami T, Ohira M, Muto H, Sakai M. Indentation contact behavior of copper–graphite particulate composites: Correlation between the contact parameters and the electrical resistivity. *Carbon N Y* 2008;46:671–8. <https://doi.org/10.1016/j.carbon.2008.01.023>.
- [53] Futami T, Ohira M, Muto H, Sakai M. Contact/scratch-induced surface deformation and damage of copper-graphite particulate composites. *Carbon N Y* 2009;47:2742–51. <https://doi.org/10.1016/j.carbon.2009.05.034>.
- [54] Rajakumar N, Subramanian K, Sozhan G, Ramasamy K. Tribological studies of the sintered bronze—tungsten disulfide composites. *Mater Res Express* 2019;6:086568. <https://doi.org/10.1088/2053-1591/ab1a8c>.